RSC Advances

PAPER

Cite this: *RSC Adv.*, 2019, **9**, 13561

The magnetism of 1T-MX_2 (M = Zr, Hf; X = S, Se) monolayers by hole doping†

Hui Xiang,[*abc] Bo Xu,[d] Weiqian Zhao,[a] Yidong Xia,[b] Jiang Yin,[b] Xiaofei Zhang[a] and Zhiguo Liu[*b]

Received 17th February 2019
Accepted 16th April 2019

DOI: 10.1039/c9ra01218d

rsc.li/rsc-advances

The magnetism of hole doped 1T-MX_2 (M = Zr, Hf; X = S, Se) monolayers is systematically studied by using first principles density functional calculations. The pristine 1T-MX_2 monolayers are semiconductors with nonmagnetic ground states, which can be transformed to ferromagnetic states by the approach of hole doping. For the unstrained monolayers, the spontaneous magnetization appears once above the critical hole density (10^{14} cm^{-2}), where the p orbital of S or Se atoms contributes the most of the magnetic moment. As the tensile strains exceed 4%, the magnetic moments per hole of ZrS_2 and HfS_2 monolayers increase sharply to a saturated value with increasing hole density, implying obvious advantages over the unstrained monolayers. The phonon dispersion calculations for the strained ZrS_2 and HfS_2 monolayers indicate that they can keep the dynamical stability by hole doping. Furthermore, we propose that the fluorine atom modified ZrS_2 monolayer could obtain stable ferromagnetism. The magnetism in hole doped 1T-MX_2 (M = Zr, Hf; X = S, Se) monolayers has great potential for developing spintronic devices with desirable applications.

1 Introduction

Since atomically thick transition metal dichalcogenides (TMDCs) can be synthesized in experiments, they have been considered as promising candidates for next generation nanoelectronics, due to their interesting physical phenomena, including the quantum spin Hall effect, valley polarization, two-dimensional superconductivity, and so on.[1–8] Zirconium and hafnium dichalcogenides MX_2 (M = Zr, Hf; X = S, Se), one group of TMDCs, have attracted attention due to their unique electrical and optoelectronic properties.[9–13] ZrS_2 nanobelt photodetectors have demonstrated excellent electrical transport and high-performance photoconductivity, such as a response time of ~2 μs, responsivity of 7.1×10^5 A W^{-1}, and a quantum efficiency of 1.8×10^8%.[10] The acoustic phonon limited room-temperature electron mobility of MX_2 (M = Zr, Hf; X= S, Se) monolayers can be above 1200 cm^2 V^{-1} s^{-1}, which is much higher than that of MoS_2 (340 cm^2 V^{-1} s^{-1}), SnS_2 (306 cm^2 V^{-1} s^{-1}) and some other TMDCs.[11] As we know, spintronic devices play an important role in promising applications in information storage and processing. Significantly, previous studies have found that the magnetism based on the sp states of nonmetal elements has some obvious advantages, such as stronger long-range exchange coupling interactions and no clustering of magnetic ions, which generally enhance the electronic spin transport and spin-polarization.[14,15] The efficient electron transport characteristic in MX_2 (M = Zr, Hf; X = S, Se) monolayers would be important in spin electronics. Unfortunately, most two dimensional (2D) TMDCs, including MX_2 (M = Zr, Hf; X = S, Se), are naturally nonmagnetic, which largely limits their applications.

It is generally that the magnetic and spin polarization strongly depends on the electronic structures near the Fermi level (E_F). Once the density of states (DOS) near the Fermi level is large enough to satisfy the "Stoner criterion",[16] the spin splitting would occur. In past years, the electronic structures can be tunable by using several methods. Of particular concern is that the strain engineering is commonly used to tune the electronic structures in 2D TMDCs, which is because of their superior elasticity and structural stability to one atomic thick crystals and bulk in a wide range of strain.[17–19] By applying strains, previous studies predicted the switched ferromagnetism in TMDCs monolayers, such as VX_2 and NbX_2 (X = S, Se), and CrX_2 (X = Se, Te). Besides, carrier doping is considered as another effective approach to modulate E_F. Cao *et al.*[20] and Huang *et al.*[21] reported the theoretical investigation of magnetism in GaSe and silicon phosphides, respectively. We also systematically studied

[a]School of Mathematics and Physics, Hubei Polytechnic University, Huangshi, 435003, China. E-mail: hxiang0717@163.com
[b]National Laboratory of Solid State Microstructures, Department of Materials Science and Engineering, Nanjing University, Nanjing, 210093, China. E-mail: liuzg@nju.edu.cn
[c]School of Chemistry and Chemical Engineering, Wuhan University of Science and Technology, Wuhan, 430081, China
[d]School of Sciences, Key Laboratory of Biomedical Functional Materials, China Pharmaceutical University, Nanjing, 211198, China

† Electronic supplementary information (ESI) available. See DOI: 10.1039/c9ra01218d

the strain tunable magnetism of SnX_2 (X = S, Se) and graphene-like C_2N by hole doping in previous work.[22,23] To obtain the carrier doping, there are several approaches availably in experiments, such as electric-field control in field effect transistors (FETs),[24–26] introducing impurity atoms or vacancies,[27] adatom decoration in 2D nanosheets[28,29] and so on.

For MX_2 (M = Zr, Hf; X = S, Se) monolayers, previous studies have indicated that electronic structures can be effectively tuned by mechanical strain.[30,31] In this work, strain engineering and carrier doping are both employed. We report the realization of the magnetism on hole doped 1T-MX_2 (M = Zr, Hf; X = S, Se) monolayers on the basis of first-principle calculations. We find that four monolayers can be magnetized by hole doping. When the strains reach 4%, the magnetic moments of hole doped disulfides can be obviously increased to constants with lower critical hole density in comparison with the unstrained states. Moreover, fluorine doped ZrS_2 monolayer is a p-type semiconductor, meaning that the fluorination is one of effective ways to realize hole doping. We also predicted that the fluorinated ZrS_2 monolayer shows stable ferromagnetic property. Therefore, ZrS_2 and HfS_2 monolayers could be considered as viable candidates for spintronic devices.

2 Computational methods

To study the electronic and magnetic properties of the MX_2 (M = Zr, Hf; X = S, Se) monolayers, density functional theory (DFT) calculations were performed using the Projector-Augmented Wave (PAW) pseudopotential implementation of the Vienna Ab Initio Simulation Package (VASP).[32–34] Electron exchange and correlation effects were described by the generalized gradient approximation (GGA) functional of Perdew–Burke–Ernzerhof (PBE) formula.[35] The energy cutoff for the plane-wave basis was set as 550 eV on the $11 \times 11 \times 1$ Monkhorst–Pack k-point grid for all simulations. The convergence threshold was 1×10^{-5} eV for the electronic self-consistent field iterations. The atomic positions were optimized until the maximum Hellman–Feynman force on each atom was less than 10^{-2} eV Å^{-1}. A vacuum spacing of 20 Å was placed to avoid the interactions between the monolayers and its periodic images. Moreover, to examine the dynamical stability of strained MX_2 monolayers by hole doping, the phonon dispersions were calculated by density functional perturbation theory (DFPT) in VASP & phonopy.

3 Results and discussion

3.1 Geometric structures

The hexagonal crystal structures of 1T-MX_2 (M = Zr, Hf; X= S, Se) monolayers with a globally D_{3d} point-group symmetry are covalently bonded by octahedrally-coordinated sandwich layers, where the central M atom in the octahedron bonds to six nearest-neighbor X atoms located in the top and bottom sublayers, as shown in Fig. 1. Each primitive hexagonal unit cell, marked by the rhombus with red dashed line, contains one transition metal and two chalcogenide atoms. Before investigating the strain effect on magnetic properties of MX_2 monolayers, we first relaxed the lattice constants and atomic

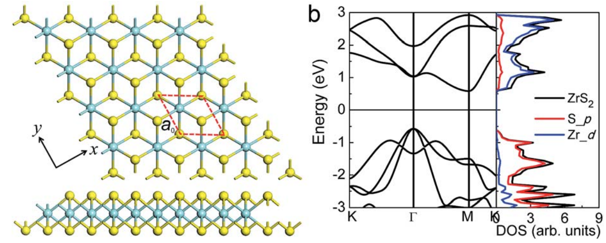

Fig. 1 (a) The crystal structures of optimized 1T-MX_2 (M = Zr, Hf; X = S, Se) monolayers, where the images above and below represent the top and side view, respectively. The green and yellow balls represent the transition metals and chalcogenide atoms, respectively. The red dotted rhombus represents the unit cell. (b) The band structure and DOS of ZrS_2 monolayer. The red and blue lines in the right image represent the contribution of the 3p orbital of S atoms and the 4d orbital of Zr atom, respectively.

positions to obtain the optimized geometric structures. The optimized geometric parameters of MX_2 monolayers are listed in Table 1, which are excellently consistent with the values previously reported,[31,36] and slightly larger than that of bulk TMDCs.[37] Besides, we also studied the mechanical properties of MX_2 monolayers. The elastic stiffness constants C_{11} (along the x direction) and Poisson ratio ν are listed in Table 1. The value of C_{11} are about 64–80 N m^{-1}, which are much smaller than that of graphene (352 N m^{-1}), BN (290 N m^{-1}), MoS_2 (130 N m^{-1}), and $MoSe_2$ (108 N m^{-1}), respectively.[38,39] Therefore, 1T-MX_2 (M = Zr, Hf; X = S, Se) monolayers perform better flexibility along the in-plane direction.

3.2 Electronic structures

Electronic properties of MX_2 (M = Zr, Hf; X = S, Se) monolayers are also studied by employing PBE functional. Four compounds of MX_2 monolayers are indirect band-gap semiconductors, and the valence band maximum (VBM) and conduction band minimum (CBM) in the Brillouin zone are located at the Γ and M points, respectively. The band gaps E_g listed in Table 1 predicted that the E_g of Zr and Hf disulfides are nearly twice that of corresponding diselenides, respectively. Herein, we take an example of the band structure and DOS of ZrS_2, as shown in Fig. 1(b), others are depicted in Fig. S1.† The VBM and CBM are mainly attributed to the 3p orbital of S atoms and the 4d orbital of Zr atoms, respectively. The small dispersion near the Γ point indicates the outstanding electron mobility, which is in accordance with the previous values reported by Zhang *et al.*[11] The electronic structures of three other MX_2 monolayers are similar to that of ZrS_2.

3.3 Magnetism of MX_2 monolayers

It is clear that MX_2 (X = Zr, Hf; X = S, Se) monolayers have excellent mechanical and electronic properties, such as the superior flexibility and carrier mobility, which indicates their promising applications in electronic and optoelectronic devices. To extend their applications in spintronic devices, we systematically studied the magnetism of MX_2 monolayers by using carrier doping.

Table 1 The optimized geometric parameters of MX_2 monolayers, including in-plane lattice constants a_0, the monolayer chalcogenide heights (h), the nearest atomic distances of the M–X (d_{M-X}), and the bond angle of the X–M–X (θ_{X-M-X}) are summarized. Besides, the band gaps E_g are also listed

Materials	a_0 (Å)	a_0 (Å) (exp. bulk)	h (Å)	d_{M-X} (Å)	θ_{X-M-X} (°)	C_{11} (N m^{-1})	ν	E_g (eV)
ZrS_2	3.684 (3.691[a])	3.66[b]	2.915	2.578	88.82	75	0.20	1.16
$ZrSe_2$	3.797 (3.806[a])	3.76[b]	3.175	2.707	90.92	64	0.21	0.57
HfS_2	3.647 (3.646[a])	3.62[b]	2.888	2.553	88.85	80	0.18	1.44
$HfSe_2$	3.772 (3.771[a])	3.73[b]	3.147	2.687	90.84	69	0.19	0.74

[a] Ref. 36. [b] Ref. 37.

By using hole injection to tune the Fermi level, MX_2 (M = Zr, Hf; X = S, Se) monolayers can be modulated to be p-type semiconductors with the relatively large E_F, caused by the changes of S_p or Se_p orbitals, and consequently would provide the possibility to develop a spontaneous ferromagnetism. We applied hole doping to investigate the possible ferromagnetism in MX_2 monolayers. Fig. 2 shows the local magnetic moment per hole and the spin-polarization energy per hole ΔE_p (*i.e.*, the total energy difference between the spin-polarized state and non-spin-polarized state normalized by the number of holes) under the various hole density n_h. At the nonmagnetic ground state, both the magnetic moment and ΔE_p are nearly zero. Once above the critical hole density n_{hc}, the magnetic moments and the absolute values of ΔE_p firstly increase and then gradually return to zero. When the n_h are around 2.5 × 10^{14} cm^{-2}, the maximum values of magnetic moment are about 0.7, 0.26, 0.61 and 0.24 μ_B per hole for ZrS_2, $ZrSe_2$, HfS_2 and $HfSe_2$, respectively, which are mainly contributed by the p orbitals of S or Se atoms. The minimum of ΔE_p are about −15, −7, −13 and −8 meV per hole for ZrS_2, $ZrSe_2$, HfS_2 and $HfSe_2$, respectively. Therefore, by using hole doping, both the magnetic moments and ferromagnetic stabilities at ground state indicate that ZrS_2 (HfS_2) would have superior characteristics in comparison with $ZrSe_2$ ($HfSe_2$).

For the unstrained structures, the critical hole densities are about 1.6 × 10^{14} cm^{-2} and 1.8 × 10^{14} cm^{-2} for ZrS_2 and HfS_2, respectively. The high hole density would bring unexpected uncontrollability and difficulty for their practical applications. And even worse, the nonzero magnetic moment can be existed in the very narrow range, which would be limited their potential in spintronics. As we known, in most 2D materials, strain engineering is one of effective approaches to modulate the electronic structures, due to their excellent elasticity and structural stability in a wide range of strain. Recently, we reported the effects of biaxial strain on the electronic structures for SnS_2 and $SnSe_2$ monolayers.[22] It predicted an obvious increment of the DOS near the valence band edges, resulting in the reduction of the critical hole density to ~10^{13} cm^{-2} when the strain reached 4% (6%) in SnS_2 ($SnSe_2$). Based on the magnetism of MX_2 (M = Zr, Hf; X = S, Se) monolayers displayed above, the biaxial in-plane strains [2%, 10%], with an increment of 2%, were applied to ZrS_2 and HfS_2. Fig. 3 shows the evolution of the DOS near the valence band edges. It is clear that the DOS near the VBM increases with increasing the strain. While the strain exceeds 4%, the values of E_F are close to VBM, and the Mexican-hat-like dispersions are formed around Γ points. Such large E_F would lead to a ferromagnetic state with the lower hole density in comparison with the unstrained structure.

The local magnetic moments of ZrS_2 and HfS_2 under the biaxial strains in the range of [0%, 10%] are shown in Fig. 4(a) and (b), respectively. Compared with the unstrained structures, the magnetic moment per hole increases with the increment of the strains, more importantly, the critical hole density of the ferromagnetic transition dramatically reduces. When the strains exceed 4%, provided $n_h < 1.0 \times 10^{14}$ cm^{-2}, the magnetic moment per hole increases sharply to a saturated value of 1.0 μ_B per hole with having a plateau region. For example, applying the strain of 6%, the critical hole densities are about 7 × 10^{13} cm^{-2} and 5 × 10^{13} cm^{-2} for ZrS_2 and HfS_2, respectively, which are much lower than those of unstrained structures. The saturated magnetic moment per hole can be maintained till the hole

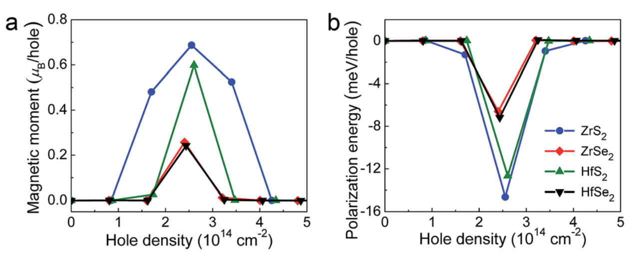

Fig. 2 Hole density dependence of the magnetic moment per hole (a) and the spin polarization energy per hole (b).

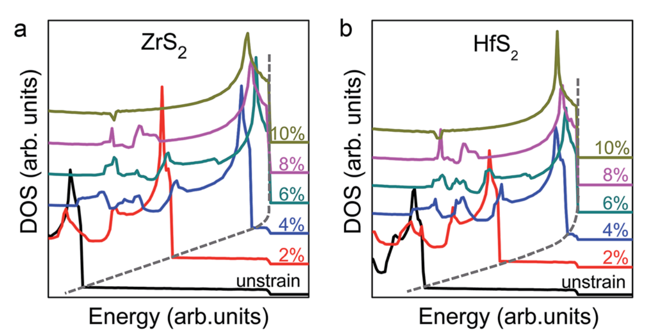

Fig. 3 The evolution of DOS near the valence band edges for ZrS_2 (a) and HfS_2 (b) with the strain from 2% to 10%, where the black lines represent the unstrained structures.

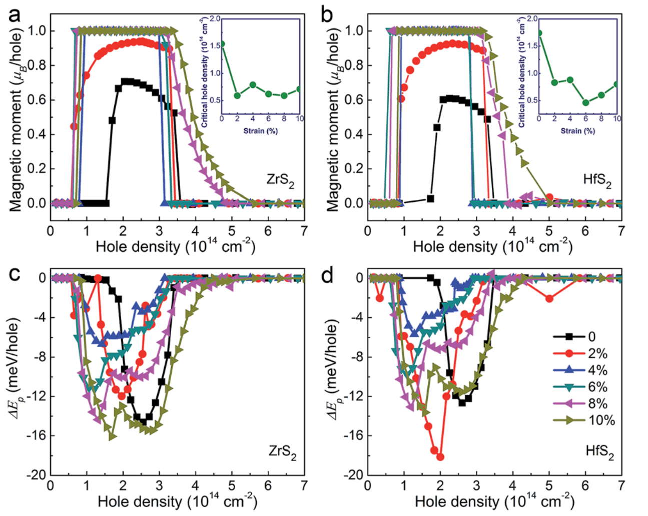

Fig. 4 Hole densities dependence of the magnetic moments per hole of ZrS_2 (a) and HfS_2 (b) under biaxial strains in the range from 2% to 10%. (c) and (d) represent spin polarization energies per hole of ZrS_2 and HfS_2, respectively, where the black dotted lines represent the unstrained structures.

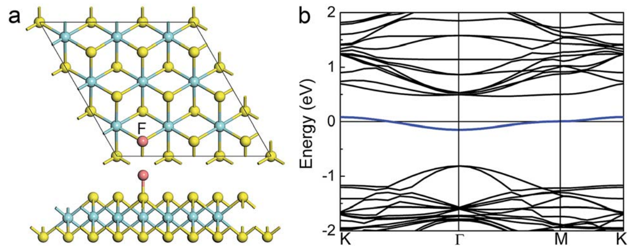

Fig. 5 (a) Crystal structures of optimized F_ZrS_2 monolayer, where the images above and below represent the top and side view, respectively. The red ball absorbed on the top of the sulfide atom represents the fluorine atom. (b) The band structure of F_ZrS_2 monolayer. The isolated blue line represents the motion from the valence band in pristine ZrS_2 monolayer. The Fermi level is set to zero.

density is up to around 3.0×10^{14} cm^{-2}, and then ZrS_2 and HfS_2 return to nonmagnetic states.

Next we check the stabilities of spin polarization energies of the strained structures, as shown in Fig. 4(c) and (d). At the nonmagnetic states, ΔE_p are nearly zero. Once above the critical hole densities, the spontaneous magnetization occurs, $\Delta E_p < 0$. Increasing the strain strength from 0 to 10%, the spin polarization energy of ZrS_2 and HfS_2 monolayers at the same hole density does not significantly change, meaning that the similar magnetic transitions can be obtained under the strains. As the absolute values of spin polarization energy are not large enough to keep the ferromagnetic states under the room temperature, ZrS_2 and HfS_2 monolayers would be appropriate in the low-temperature spintronic devices.

Using common FETs in experiments, the concentration of hole can be achieved accurately. Except for that case, controlling impurity atoms or vacancies is another effective method to regulate the concentration of carrier, for the decorated atoms in 2D sheets generally change the DOS near the Fermi level, and generally modulate intrinsic semiconductors to n/p type.[40] Therefore, the magnetism induced by introducing impurity atoms or vacancies has also attracted considerable attentions over past years. Herein, take an example of ZrS_2 monolayer, a fluorine atom is adsorbed on the top of S atoms in $3 \times 3 \times 1$ ZrS_2 supercell, termed as F_ZrS_2, the electronic and magnetic properties are studied.

The geometric structure of F_ZrS_2 monolayer was first optimized, as shown in Fig. 5(a). The lattice parameters are 11.07 Å, almost three times of the pristine primitive cell. The bond length of F–S is 1.69 Å. To check the stability of the F_ZrS_2 monolayer, the energy of adsorption (ΔE) was calculated as

$$\Delta E = E(\mathrm{F\_ZrS_2}) - E(\mathrm{ZrS_2}) - \frac{1}{2}E(\mathrm{F_2}) \tag{1}$$

where $E(\mathrm{F\_ZrS_2})$ and $E(\mathrm{ZrS_2})$ are the energies of ZrS_2 with and without F adsorption, respectively. $E(\mathrm{F_2})$ is the energy of singe-molecule F_2. By using PBE formula, ΔE is about −0.70 eV, indicating that the fluorine adsorption in ZrS_2 monolayer is feasible.

Then the band structure of F_ZrS_2 is displayed in Fig. 5(b). Compared with the pristine ZrS_2 monolayer, it is clear that one isolated band across the Fermi level is from the valence band, indicating p-type doping. Moreover, the width of isolated band is about 0.23 eV. Once the special band is occupied by large amounts of electrons, according to Stoner criterion, the spin splitting near the Fermi level would occur. To confirm whether the magnetism exists, we calculated the local magnetic moment and the spin-polarization energy of F_ZrS_2 monolayer. The magnetic moment is about 0.68 μ_B, which is co-contributed mainly by the p orbitals of F atoms, and the adjacent S_p and Zr_d atoms. Besides, a spin distribution is asymmetric near the Fermi level, indicating that the magnetic moment mainly originates from the hybridization of p_z orbitals of F and S atoms, and the d_{z^2} orbitals of the Zr atoms. The spin-polarization energy is about 25 meV, meaning the stable spin-polarization state. Moreover, ZrS_2 monolayer is one of many TMDCs. Materials such as HfS_2, $ZrSe_2$ and $HfSe_2$ monolayer have similar crystal and electronic structures, as shown in Fig. 1 and S1.† The fluorine doping in this family would offer a great opportunity to explore magnetic phenomena in 2D materials, which also provides another effective way to design spintronic devices in experiments.

3.4 Stability of MX_2 monolayers

The stability of hole doped MX_2 monolayers is crucial for their applications on magnetism. So, we have also carried out the phonon dispersions to study their dynamical stabilities, as shown in Fig. 6. The phonon dispersions of unstrained ZrS_2 and HfS_2 monolayers are firstly considered for the better comparison. All positive frequency indicates dynamic stability for unstrained structures. Then applying the strain of 6%, the stability of ZrS_2 and HfS_2 monolayers is studied. It is clear that no imaginary frequency is found under the strain, meaning that the approach of modulating electronic structures by applying tensile strain would be obtained theoretically. At the hole

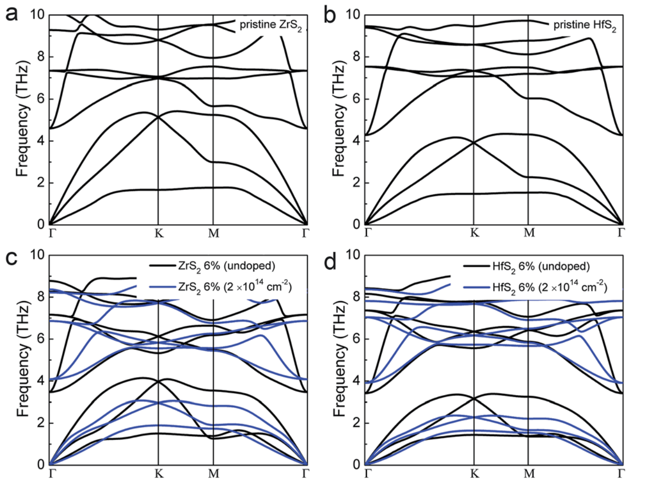

Fig. 6 Phonon dispersion calculations of ZrS_2 and HfS_2 monolayers. (a) and (b) represent the unstrained states; (c) and (d) represent the strain at 6%. The black and blue lines present the undoped and hole doped states, respectively, where the hole densities are both around 2.0×10^{14} cm^{-2}.

density of around 2.0×10^{14} cm^{-2}, large enough to induce magnetism in ZrS_2 and HfS_2 monolayers under the tensile strain of 6%, there is still no imaginary frequency, except the frequency softening comparing to the strained ZrS_2 and HfS_2 monolayers without doping. Therefore, these results indicate that hole doping in strained ZrS_2 and HfS_2 monolayers has negligible effect on their structural stabilities, and will provide feasible theoretical predictions for practical applications in spintronic devices.

4 Conclusions

In summary, using first-principle calculations, we have predicted the ferromagnetism of hole doped 1T-MX_2 (M = Zr, Hf; X = S, Se) monolayers by strain engineering. Four pristine MX_2 monolayers are nonmagnetic semiconductors with indirect band-gaps. We first demonstrate that hole doping induces tunable ferromagnetic properties in MX_2 monolayer. This carrier-tunable magnetism is tightly correlated with the p orbital of S or Se atoms. When tensile strains are applied to dichalcogenides, the critical hole density can reduce to 5×10^{13} cm^{-2}, and keep the ferromagnetic states till the hole density up to 3×10^{14} cm^{-2}, which would attribute to the enlarged DOS near the Fermi energy. Moreover, the magnetism of fluorine doped ZrS_2 monolayer is studied. Band structure shows that F_ZrS_2 is a p-type semiconductor, which confirms the hole doping. The magnetic moment and spin-polarization energy indicate that fluorine doped ZrS_2 monolayer can be modulated to stable magnetic states. The phonon dispersions of the strained ZrS_2 and HfS_2 monolayers indicate the structural stability by hole doping. Therefore, the hole doped MX_2 monolayers will provide an achievable idea for 2D functional materials in spintronics.

Conflicts of interest

There are no conflicts to declare.

Acknowledgements

This work was supported by the Fundamental Research Funds for the Central Universities, a Project Funded by the Priority Academic Program Development of Jiangsu Higher Education Institutions (PAPD). We are grateful for the support of NSFC (51672126). The calculations were performed on parallel computers at the High Performance Computing Center (HPCC) of Nanjing University.

References

1 K. F. Mak, C. Lee, J. Hone, J. Shan and T. F. Heinz, Atomically thin MoS_2: a new direct-gap semiconductor, *Phys. Rev. Lett.*, 2010, **105**, 136805.
2 J. N. Coleman, M. Lotya, A. O'Neill, S. D. Bergin, P. J. King, U. Khan, K. Young, A. Gaucher, S. De, R. J. Smith, I. V. Shvets, S. K. Arora, G. Stanton, H.-Y. Kim, K. Lee, G. T. Kim, G. S. Duesberg, T. Hallam, J. J. Boland, J. J. Wang, J. F. Donegan, J. C. Grunlan, G. Moriarty, A. Shmeliov, R. J. Nicholls, J. M. Perkins, E. M. Grieveson, K. Theuwissen, D. W. McComb, P. D. Nellist and V. Nicolosi, Two-Dimensional Nanosheets Produced by Liquid Exfoliation of Layered Materials, *Science*, 2011, **331**, 568.
3 K. F. Mak, K. He, J. Shan and T. F. Heinz, Control of valley polarization in monolayer MoS_2 by optical helicity, *Nat. Nanotechnol.*, 2012, **7**, 494.
4 X. Qian, J. Liu, L. Fu and J. Li, Quantum spin Hall effect in two-dimensional transition metal dichalcogenides, *Science*, 2014, **346**, 1344–1347.
5 Y. Saito, T. Nojima and Y. Iwasa, Highly crystalline 2D superconductors, *Nat. Rev. Mater.*, 2016, **2**, 16094.
6 G. Wang, A. Chernikov, M. M. Glazov, T. F. Heinz, X. Marie, T. Amand and B. Urbaszek, Colloquium: Excitons in atomically thin transition metal dichalcogenides, *Rev. Mod. Phys.*, 2018, **90**, 021001.
7 J. Zhou, J. Lin, X. Huang, Y. Zhou, Y. Chen, J. Xia, H. Wang, Y. Xie, H. Yu, J. Lei, D. Wu, F. Liu, Q. Fu, Q. Zeng, C.-H. Hsu, C. Yang, L. Lu, T. Yu, Z. Shen, H. Lin, B. I. Yakobson, Q. Liu, K. Suenaga, G. Liu and Z. Liu, A library of atomically thin metal chalcogenides, *Nature*, 2018, **556**, 355–359.
8 Z. Hu, Z. Wu, C. Han, J. He, Z. Ni and W. Chen, Two-dimensional transition metal dichalcogenides: interface and defect engineering, *Chem. Soc. Rev.*, 2018, **47**, 3100–3128.
9 K. Xu, Z. Wang, F. Wang, Y. Huang, F. Wang, L. Yin, C. Jiang and J. He, Ultrasensitive Phototransistors Based on Few-Layered HfS_2, *Adv. Mater.*, 2015, **27**, 7881–7887.
10 L. Li, X. Fang, T. Zhai, M. Liao, U. K. Gautam, X. Wu, Y. Koide, Y. Bando and D. Golberg, Electrical Transport and High-Performance Photoconductivity in Individual ZrS_2 Nanobelts, *Adv. Mater.*, 2010, **22**, 4151–4156.

11 W. Zhang, Z. Huang, W. Zhang and Y. Li, Two-dimensional semiconductors with possible high room temperature mobility, *Nano Res.*, 2014, **7**, 1731–1737.
12 X. Zhang, Z. Meng, D. Rao, Y. Wang, Q. Shi, Y. Liu, H. Wu, K. Deng, H. Liu and R. Lu, Efficient band structure tuning, charge separation, and visible-light response in ZrS_2-based van der Waals heterostructures, *Energy Environ. Sci.*, 2016, **9**, 841–849.
13 M. Zhang, Y. Zhu, X. Wang, Q. Feng, S. Qiao, W. Wen, Y. Chen, M. Cui, J. Zhang, C. Cai and L. Xie, Controlled Synthesis of ZrS_2 Monolayer and Few Layers on Hexagonal Boron Nitride, *J. Am. Chem. Soc.*, 2015, **137**, 7051–7054.
14 J. Coey, d^0 ferromagnetism, *Solid State Sci.*, 2005, **7**, 660–667.
15 H. Peng, H. Xiang, S.-H. Wei, S.-S. Li, J.-B. Xia and J. Li, Origin and enhancement of hole-induced ferromagnetism in first-row d^0 semiconductors, *Phys. Rev. Lett.*, 2009, **102**, 017201.
16 A. Mielke and H. Tasaki, Ferromagnetism in the Hubbard model, *Commun. Math. Phys.*, 1993, **158**, 341–371.
17 Y. Ma, Y. Dai, M. Guo, C. Niu, Y. Zhu and B. Huang, Evidence of the existence of magnetism in pristine VX_2 monolayers (X = S, Se) and their strain-induced tunable magnetic properties, *ACS Nano*, 2012, **6**, 1695–1701.
18 Y. Zhou, Z. Wang, P. Yang, X. Zu, L. Yang, X. Sun and F. Gao, Tensile strain switched ferromagnetism in layered NbS_2 and $NbSe_2$, *ACS Nano*, 2012, **6**, 9727–9736.
19 X. Feng, S. Lu, C. J. Pickard, H. Liu, S. A. T. Redfern and Y. Ma, Carbon network evolution from dimers to sheets in superconducting ytrrium dicarbide under pressure, *Communications Chemistry*, 2018, **1**, 85.
20 T. Cao, Z. Li and S. G. Louie, Tunable magnetism and half-metallicity in hole-doped monolayer GaSe, *Phys. Rev. Lett.*, 2015, **114**, 236602.
21 B. Huang, H. L. Zhuang, M. Yoon, B. G. Sumpter and S.-H. Wei, Highly stable two-dimensional silicon phosphides: Different stoichiometries and exotic electronic properties, *Phys. Rev. B: Condens. Matter Mater. Phys.*, 2015, **91**, 121401.
22 H. Xiang, B. Xu, Y. Xia, J. Yin and Z. Liu, Strain tunable magnetism in SnX_2 (X= S, Se) monolayers by hole doping, *Sci. Rep.*, 2016, **6**, 39218.
23 Z. Liang, B. Xu, H. Xiang, Y. Xia, J. Yin and Z. Liu, Carrier-tunable magnetism in two dimensional graphene-like C_2N, *RSC Adv.*, 2016, **6**, 54027–54031.
24 K. F. Mak, K. He, C. Lee, G. H. Lee, J. Hone, T. F. Heinz and J. Shan, Tightly bound trions in monolayer MoS_2, *Nat. Mater.*, 2012, **12**, 207.
25 Y. Zhang, T. Oka, R. Suzuki, J. Ye and Y. Iwasa, Electrically switchable chiral light-emitting transistor, *Science*, 2014, **344**, 725–728.
26 S. Lu, W. Ma, G. Jin, Q. Zeng, X. Feng, T. Feng, H. Liu, S. Meng, S. A. T. Redfern and B. Yang, A combined experimental and theoretical investigation of donor and acceptor interface in efficient aqueous-processed polymer/nanocrystal hybrid solar cells, *Sci. China: Chem.*, 2018, **61**, 437–443.
27 D. J. Late, L. Bin, L. Jiajun, Y. Aiming, H. S. S. R. Matte, G. Matthew, C. N. R. Rao and V. P. Dravid, GaS and GaSe ultrathin layer transistors, *Adv. Mater.*, 2012, **24**, 3549–3554.
28 P. Manchanda, A. Enders, D. J. Sellmyer and R. Skomski, Hydrogen-induced ferromagnetism in two-dimensional Pt dichalcogenides, *Phys. Rev. B*, 2016, **94**, 104426.
29 Y. Ma, Y. Dai, M. Guo, C. Niu, L. Yu and B. Huang, Strain-induced magnetic transitions in half-fluorinated single layers of BN, GaN and graphene, *Nanoscale*, 2011, **3**, 2301–2306.
30 Y. Li, J. Kang and J. Li, Indirect-to-direct band gap transition of the ZrS_2 monolayer by strain: first-principles calculations, *RSC Adv.*, 2014, **4**, 7396–7401.
31 J. Kang, H. Sahin and F. M. Peeters, Mechanical properties of monolayer sulphides: a comparative study between MoS_2, HfS_2 and TiS_3, *Phys. Chem. Chem. Phys.*, 2015, **17**, 27742–27749.
32 G. Kresse and J. Hafner, Ab initio molecular dynamics for liquid metals, *Phys. Rev. B: Condens. Matter Mater. Phys.*, 1993, **47**, 558.
33 G. Kresse and J. Furthmüller, Efficiency of ab initio total energy calculations for metals and semiconductors using a plane-wave basis set, *Comput. Mater. Sci.*, 1996, **6**, 15–50.
34 G. Kresse and J. Furthmüller, Efficient iterative schemes for ab initio total-energy calculations using a plane-wave basis set, *Phys. Rev. B: Condens. Matter Mater. Phys.*, 1996, **54**, 11169.
35 J. P. Perdew, K. Burke and M. Ernzerhof, Generalized gradient approximation made simple, *Phys. Rev. Lett.*, 1996, **77**, 3865.
36 X. Gu and R. Yang, Phonon transport in single-layer transition metal dichalcogenides: A first-principles study, *Appl. Phys. Lett.*, 2014, **105**, 131903.
37 D. L. Greenaway and R. Nitsche, Preparation and optical properties of group IV–VI_2 chalcogenides having the CdI2 structure, *J. Phys. Chem. Solids*, 1965, **26**, 1445–1458.
38 D. Çakır, F. M. Peeters and C. Sevik, Mechanical and thermal properties of h-MX_2 (M = Cr, Mo, W; X = O, S, Se, Te) monolayers: A comparative study, *Appl. Phys. Lett.*, 2014, **104**, 203110.
39 K.-A. N. Duerloo, M. T. Ong and E. J. Reed, Intrinsic piezoelectricity in two-dimensional materials, *J. Phys. Chem. Lett.*, 2012, **3**, 2871–2876.
40 X. Zhao, P. Chen, C. Xia, T. Wang and X. Dai, Electronic and magnetic properties of n-type and p-doped MoS_2 monolayers, *RSC Adv.*, 2016, **6**, 16772–16778.

